
Int. J. Nano Dimens. 2026; 17(1) : 106-117

International Journal of Nano Dimension (IJND)

https://dx.doi.org/10.57647/j.ijnd.2026.1701.07

Original Research

# Enhanced Photocatalytic Degradation of Pharmaceutical Industrial Effluent Using $TiO_2$ and N-doped $TiO_2$ Nanoparticles Under Natural Sunlight: A Comparative Study

Neha Mallika Gurramkonda[1,*], Bala Narsaiah Tumma[1], Lakshmana Naik Ramavathu[2]

[1]*Department of Chemical Engineering, JNTU College of Engineering Anantapur, Andhra Pradesh, India*
[2]*Department of Chemical Engineering, IIT Jodhpur, Karwar, Rajasthan, India*

[*]**Corresponding author:** nehamallika.gurramkonda@gmail.com

**Article History**

Received:
29 May 2025

Revised:
25 July 2025

Accepted:
28 July 2025

Published online:
30 July 2025

Published in Issue:
2 January 2026



**Abstract:**

Despite the rapid growth of pharmaceutical industries to meet rising demand, untreated or poorly treated wastewater continues to contaminate water bodies, posing serious risks to ecosystems and human health. Conventional treatment methods often fall short in effectively addressing these complex and persistent pollutants. In this context, nanomaterials have emerged as promising candidates for advanced water purification. This study presents a novel approach by employing $TiO_2$ and nitrogen-doped $TiO_2$ (N-$TiO_2$) nanoparticles, synthesized via a simple and scalable sol-gel method, for the treatment of actual pharmaceutical industrial effluent under natural sunlight, a cost-effective and sustainable condition rarely explored in previous works. The synthesized photocatalysts were thoroughly characterized using UV, XRD, SEM, FTIR, and EDX analyses. Unlike most previous studies focused on model pollutants, this work directly addresses the degradation of real pharmaceutical wastewater by combining adsorption and photocatalysis. Higher adsorption efficiencies were observed for N-doped $TiO_2$ nanoparticles (43.77%) compared to $TiO_2$ (21.34%) after 2 hours. Photocatalytic treatment further enhanced the degradation to 57% (N-$TiO_2$) and 22% ($TiO_2$) after 3 hours under natural sunlight. The study demonstrates the potential of N-$TiO_2$ as an efficient, sunlight-driven photocatalyst for practical wastewater treatment applications, highlighting its novelty and real-world applicability.

**Keywords:** Adsorption; Doped nanoparticles; Kinetics; Pharmaceutical effluent; Photocatalysis; $TiO_2$; Wastewater treatment

**Cite this article:** Gurramkonda NM, Tumma BN, Ramavathu LN. Enhanced Photocatalytic Degradation of Pharmaceutical Industrial Effluent Using $TiO_2$ and N-doped $TiO_2$ Nanoparticles Under Natural Sunlight: A Comparative Study. Int. J. Nano Dimens. 2026;17(1): 106-117. https://doi.org/10.57647/j.ijnd.2026.1701.07

## 1. Introduction

One of the most critical ways human activities impact the environment is by releasing harmful chemicals into the air and water. In recent years, the pharmaceutical sector has emerged as a significant contributor to environmental pollution [1]. Medicinal compounds for both human and veterinary use, collectively termed pharmaceuticals, have been extensively utilized globally. Despite their presence in aquatic systems even at low concentrations, their persistent presence poses long-term ecological risks to both terrestrial organisms and marine life [2]. The contamination of pharmaceutical pollutants in drinking water arises from two sources [3], namely: (i) manufacturing processes within the pharmaceutical industry, and second, the widespread consumption and disposal of pharmaceutical products, which enter domestic and agricultural wastewater streams [4].

The pharmaceutical production process generates wastewater containing a diverse range of pollutants such

as raw materials, antibiotics, PCPs, cytotoxic waste, psychotropic substances, anti-infective drugs, antiseptics, disinfectants, chemical wastes such as heavy metals, biomedical waste such as animal and plant steroids, analgesics, lipid regulators, anti-depressants, tablets, syrups, vaccines, etc. [5, 6, 7]. These effluents are often hazardous, toxic, intensely colored, and malodorous.

Various conventional and non-conventional technologies are employed to treat such wastewater, generally categorized into: (a) Physical; (b) Chemical, and (c) Biological methods. A Comparison of the average removal efficiency of several physical/chemical treatments is shown in Table 1. Although various physical, chemical, and biological technologies exist, no single method can eliminate pharmaceutical contaminants from water sources. Therefore, integrated approaches combining two or more technologies are increasingly considered optimal for efficient treatment [8]. Similar observations were reported by Thirumavalavan et al. (2019) [9], who demonstrated enhanced photocatalytic degradation of ciprofloxacin and methylene blue using $Nd_2O_3$/ZnO-GO nanocomposites under UV light. In this context, nanomaterials have received considerable attention due to their unique physicochemical properties. Their high surface area-to-volume ratio, enhanced conductivity, photosensitivity, and structural tunability offer distinct advantages over conventional materials [10]. These nanoscale characteristics result in quantum effects and intensified surface interactions, enabling targeted pollutant removal and greater efficiency [11].

Among various nanomaterials, semiconductors like titanium dioxide ($TiO_2$) have shown great promise in the photocatalytic degradation of pharmaceutical pollutants [12]. $TiO_2$ is widely used because of its high oxidative capacity, chemical stability, non-toxicity, and cost-effectiveness [13]. Numerous studies confirm the effectiveness of $TiO_2$-based photocatalysts in degrading a wide range of pharmaceuticals under both UV and visible light irradiation.

To address the inherent limitations of pristine $TiO_2$ such as limited visible light absorption and rapid electron-hole recombination, several modification strategies have been developed. These include carbon-based doping, semiconductor coupling, and non-metal doping [14]. The comprehensive review by Huang et al. (2016) details how different doping modes (self-doping, non-metal, metal, and co-doping), preparation methods, and defect chemistries influence $TiO_2$'s band structure, charge transport, and surface active sites underscoring doping's pivotal role in extending light absorption and suppressing carrier recombination [15]. For example, carbon dot-modified $TiO_2$ has shown enhanced degradation performance against pharmaceutical residues [16]. Also, Ghasemi et al. (2024) highlight that Z- and S-scheme heterojunction designs synergistically combine spatial charge separation with strong redox potential, offering a powerful blueprint for next-generation visible-light-active photocatalysts [17]. For example, Ren et al. (2025) highlight multiple S-scheme heterojunction photocatalysts, where dual or even triple S-schemes create additional charge-transfer pathways and strong interfacial electric fields to dramatically boost visible-light–driven degradation efficiencies and suppress recombination [18]. Aswini et al. (2023) identified carbon decorated bismuth based nanomaterials as versatile, visible light active photocatalysts offering high chemical stability, low toxicity, and enhanced charge separation for the efficient degradation of organic pollutants [19]. Similarly, spherical $SrWO_4$ nanomaterials synthesized via surfactant assisted co precipitation achieved over 95% methylene blue degradation within 90 minutes, driven by hydroxyl and superoxide radicals and exhibited excellent recyclability [20]. Researchers have also reported that metal-organic frameworks (MOFs) and hybrid nanocomposites significantly enhance $TiO_2$'s photocatalytic efficiency under real wastewater conditions [21, 22]. Hybrid structures incorporating $SiO_2$ and MOFs like ZIF-8 have exhibited synergistic effects in enhancing photocatalytic dye degradation, highlighting the role of tailored support matrices [23].

Solar-driven photocatalysis, in particular, aligns with green chemistry principles, with reported degradation efficiencies exceeding 95% for compounds such as paracetamol using natural sunlight [24]. Labidi et al. (2024) further demonstrated that a visible-light-driven ZnO@NiO heterostructure supported on coal fly ash waste achieved efficient ciprofloxacin degradation-driven by hydroxyl, superoxide, and sulfate radicals and provided detailed mechanistic insights via DFT calculations and toxicity pathway analysis [25]. In addition to degrading pharmaceutical residues, certain nanomaterials exhibit dual functionality by also inhibiting resistant microbial strains [26]. Moreover, organic scaffolds like pyrazoles have shown targeted antibacterial activity, further supporting the case for multi-functional photocatalytic systems [27]. Adsorption, another potent removal process, is widely used due to its porous nature and tunable surface characteristics. Combining adsorption with photocatalysis is a promising synergistic approach, enabling improved pollutant removal, prolonged adsorbent lifespan, and enhanced treatment reliability [28, 29]. Photocatalytic degradation using $TiO_2$ involves the generation of electron-hole pairs under light irradiation, which produce reactive oxygen species (ROS)

**Table 1.** The average removal efficiency of several physicochemical treatment methods: A comparison.

| Treatment method | Sedimentation | Coagulation | Fenton | Fe-C | Flotation | Adsorption | Photo-catalysis |
|---|---|---|---|---|---|---|---|
| Average removal % | 50-80 | 50-80 | 60-95 | 60-75 | 70-85 | Around 80 | 85-99 |

https://dx.doi.org/10.57647/j.ijnd.2026.1701.07

like hydroxyl radicals (OH) and superoxide anions ($O_2^-$). Labidi et al. (2024) demonstrated that organic-radical functionalization-where surface-bound radicals generate abundant reactive oxidative species-dramatically enhances the removal of pharmaceutical residues from wastewater by providing highly reactive surface sites [30]. These ROS play a key role in breaking down pharmaceutical pollutants. However, pure $TiO_2$ suffers from rapid charge recombination and limited visible light activity. Nitrogen doping addresses this by narrowing the band gap and enhancing visible-light absorption. It also improves charge separation by introducing localized states, thereby increasing ROS generation. The degradation mechanism typically involves hydroxylation, demethylation, and ring-opening of drug molecules, depending on their chemical structure and interaction with the doped surface. For example, Cunha et al. (2013) synthesized N-doped $TiO_2$ via a sol-gel route optimized by a Box-Behnken design adjusting pH, catalyst loading, and nitrogen content to achieve 98% metoprolol degradation under simulated solar light, highlighting the critical role of process optimization in maximizing photocatalytic performance [31].

Despite breakthroughs in material modification and treatment techniques, real-world applications demand cost-effectiveness, simplicity, and environmental sustainability. Simple and cost-effective synthetic approaches, such as the sol–gel method and green plant-mediated routes, have proven highly effective for producing metal oxide nanomaterials like ZnO, $TiO_2$ with desirable surface properties and photocatalytic potential [32, 33]. In the present study, nitrogen doping was employed to enhance the visible light activity of $TiO_2$ by narrowing its band gap. This modification method is straightforward, scalable, and avoids the use of hazardous reagents. The doped material was evaluated under natural sunlight and in actual pharmaceutical wastewater, aiming to bridge the gap between laboratory-scale research and real-world applications in sustainable wastewater treatment.

## 2. Materials and Methods

### 2.1 Materials

The study utilized titanium isopropoxide, ammonia, ethanol (95%), and isopropyl alcohol, all procured from Sigma Aldrich Chemicals (India) Ltd. The reagents of analytical grade were utilized as received, without additional refining steps. Distilled water was used throughout the experimental procedures.

### 2.2 Synthesis of $TiO_2$ and N-$TiO_2$ nanoparticles

Both $TiO_2$ and N-$TiO_2$ nanoparticles were synthesized using the sol-gel method (see figure 1). The synthesis procedure for $TiO_2$ nanoparticles is detailed in [34], wherein 9 mL of titanium isopropoxide (TTIP) was added dropwise to an ethanol-water mixture under constant magnetic stirring for 4 hours at 85 °C. The resulting mixture was dried at 80 °C for 20 minutes and calcined at 400 °C for 3 hours to obtain the anatase phase. For the synthesis of N-doped $TiO_2$ nanoparticles, a similar

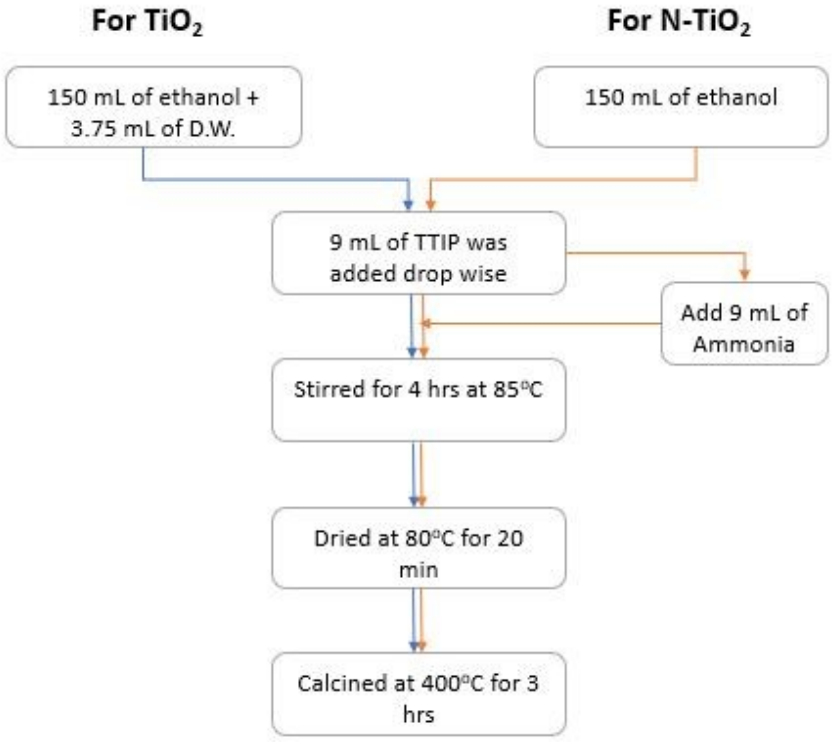


**Figure 1.** Synthesis flowchart of $TiO_2$ and N-$TiO_2$ nanoparticles via Sol-Gel processing.

https://dx.doi.org/10.57647/j.ijnd.2026.1701.07

protocol was followed with the modification of adding 5 mL of ammonia dropwise as a nitrogen source to the ethanol-TTIP solution. The mixture was stirred under identical conditions and subsequently subjected to the same drying and calcination steps. The introduction of ammonia facilitates nitrogen incorporation into the $TiO_2$ lattice, potentially enhancing its photocatalytic performance [35].

### 2.3 Collection and storage of the sample

The real industrial effluent from a pharmaceutical industry's treatment plant (the industry requested anonymity) was sampled from a homogeneous tank. Before collecting, the sampling vessel underwent thorough cleaning and rinsing with distilled water. Subsequently, it was rinsed with the sample itself. The sample collected was then stored at a temperature of 4 °C [36]. The pharmaceutical sample was analyzed for adsorption followed by photocatalytic treatment that is carried out under natural sunlight using $TiO_2$ and N-$TiO_2$ as catalysts by observing the effect of time [37].

### 2.4 Experimental set-up

100 mL of pharmaceutical solutions with a concentration of 100 volume percent are prepared in two conical flasks. In these, 0.2 g of adsorbent is added and kept inside the orbital shaker for dark adsorption for 2 hours followed by natural sunlight exposure for 3 hours (see figure 2). The samples drawn at specific intervals of time are collected with the help of micropipettes. A spectrophotometer (SHIMADZU UV-1800) is utilized to measure and calculate the percentage absorbance values at the wavelength corresponding to maximum absorbance, ($\lambda_{max}$ = 310 nm). The pharmaceutical solution concentrations were measured for every time interval until equilibrium was reached and % removal efficiency can be calculated as follows [38]:

$$\text{Removal } (\%) = \frac{(C_i - C_f)}{C_i} \times 100 \qquad (1)$$

where $C_i$ and $C_f$ are the initial and final concentrations of the samples respectively.

### 2.5 Calibration curve

Stock solutions in water were prepared, and a calibration curve of Concentration Vs. absorbance is made first. For this, the concentrations of the sample were prepared as 10, 20, 30, 40, 50, 60, 70, 80, 90, and 100 volume percent, as shown in the figure 3. The UV spectrophotometer ($\lambda_{max}$ = 310 nm) was utilized to determine their percentage absorbances (refer figure 4).

## 3. Results and discussion

### 3.1 UV-Vis Spectroscopic analysis

Nitrogen-doped $TiO_2$ exhibits a red-shifted absorption edge at approximately 403 nm, as observed in figure 5. In contrast, the normal absorbance for $TiO_2$ alone typically falls in the range of the near UV region. This shift indicates a notable narrowing of the band gap due to the incorporation of nitrogen, which introduces mid-gap states between the valence and conduction bands. Such doping facilitates enhanced absorption in the visible spectrum, thereby improving the photocatalytic performance of N-$TiO_2$ under natural sunlight.

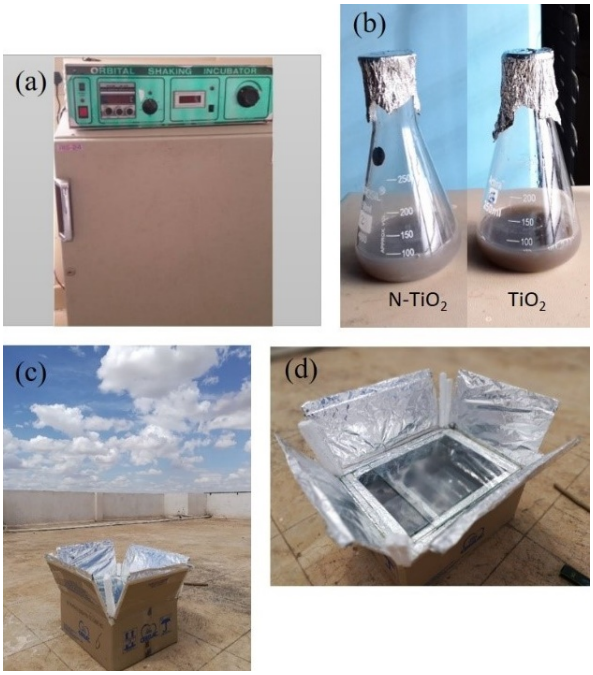


**Figure 2.** Experimental set up (a) 0.2 g of $TiO_2$ and N-$TiO_2$ nanoparticles of 100 v/v initial sample concentration kept in an orbital shaker, (b) after 2 hours of adsorption, (c) and (d) Adsorbed samples kept under sunlight for 3 hours.

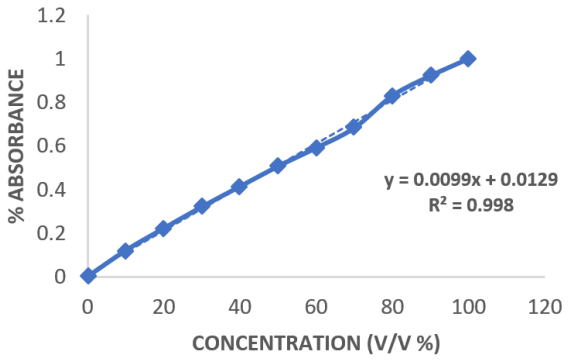


**Figure 3.** Calibration curve for pharmaceutical samples at maximum absorbance (310 nm).

### 3.2 FTIR analysis

In figure 6, a sharp peak is observed at 772 $cm^{-1}$, which corresponds to Ti-O bending. Another noticeable peak at the 1500-1600 $cm^{-1}$ region is observed, which corresponds to Ti-OH stretching. A broad peak at the 3200-3600 $cm^{-1}$ region belongs to the OH group. Hence, the synthesized nanoparticles confirm the presence of $TiO_2$ bonds. Like $TiO_2$ nanoparticles, N-$TiO_2$ has exhibited noticeable peaks at the same regions as in $TiO_2$, but with an extra peak. The intense peak at 1600 $cm^{-1}$ region is observed which corresponds to N-H stretching. Hence,

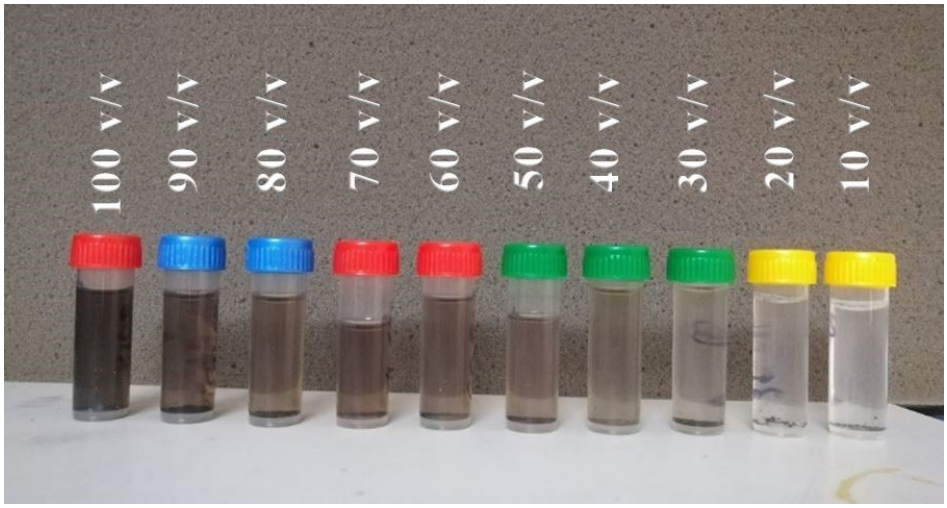


**Figure 4.** Calibration samples for pharmaceutical samples at maximum absorbance (310 nm).

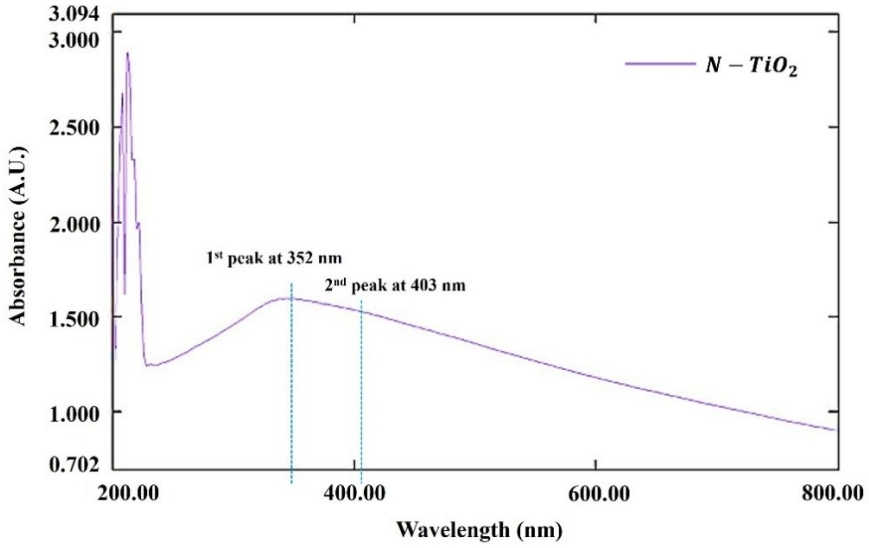


**Figure 5.** UV spectrum of N-$TiO_2$ nanoparticles.

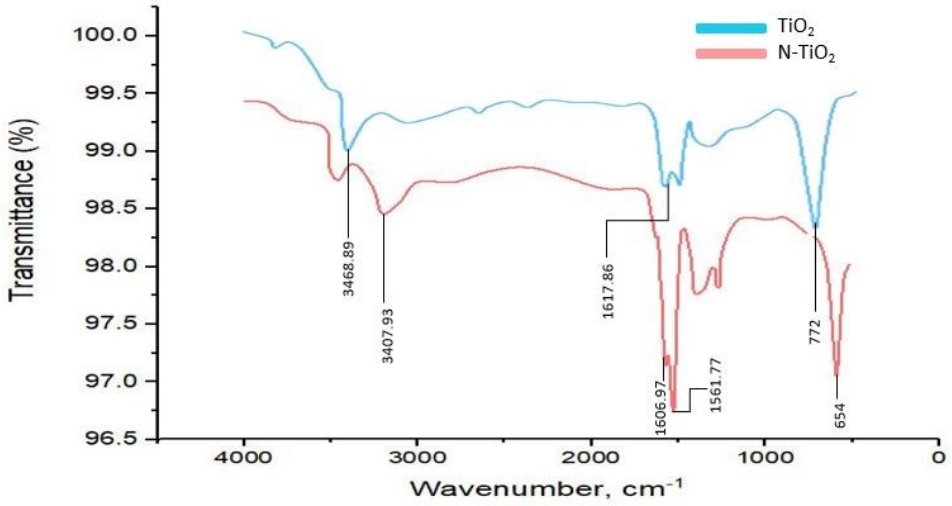


**Figure 6.** FTIR analysis of $TiO_2$ and N-$TiO_2$ nanoparticles.

https://dx.doi.org/10.57647/j.ijnd.2026.1701.07

it is concluded that the synthesized nanoparticles have N-H bonds as well as $TiO_2$ bonds. Table 2 represents the FTIR peak table for all the main peaks present in the synthesized nanoparticles.

### 3.3 X-Ray diffraction (XRD) analysis

A powder X-ray diffraction (pXRD) analysis was conducted to determine the crystallographic properties of the synthesized N-$TiO_2$ nanoparticles. The resulting diffractogram (figure 7) revealed distinct peaks at $2\theta$ values of 25.41°, 27.41°, 38.23°, 39.1°, 45.41°, 48.24°, 49.24°, 53.75°, 55.22°, 63.27°, 70.08°- which corresponds to the (1 0 1), (1 1 1), (0 0 4), (2 1 1), (2 2 0), (2 0 0), (2 1 2), (3 0 1), (2 1 1), (0 2 4), and (4 0 0) planes of the anatase $TiO_2$ phase. These results confirm that nitrogen doping did not alter the crystal structure, which remains tetragonal anatase. The crystallite size of the N-$TiO_2$ nanoparticles was calculated using the Debye–Scherrer equation (Eq. (2)), yielding an average diameter of 61.26 nm (Table 3).

$$\text{Debye-Scherrer formula}: D = \frac{K\lambda}{\beta \cos\theta} \qquad (2)$$

where, $D$ = Crystallite size; $K$ = Shape factor (typically 0.9 for spherical crystals); $\lambda$ = X-ray wavelength (usually 1.54056 Å for Cu Kα radiation); $\beta$ = Full width at half maximum (FWHM) of the peak in radians; $\theta$ = Bragg angle in radians. For comparison, the crystallite size of undoped $TiO_2$, for previously reported work has been calculated in Table 4 [39], was found to be 21.38 nm. This significant increase in crystallite size upon doping may be attributed to the lattice strain or defect states introduced by nitrogen incorporation.

**Table 2.** FTIR peak table.

| Functional group | Frequency ($cm^{-1}$) |
|---|---|
| Water OH stretch | 3700-3100 (s) |
| Alcohol OH stretch | 3600-3200 broad (s) |
| Amine N-H stretch | 3500-3300 (w) |
| $CH_2$ bend | 1480-1400 (m) |
| Bending nodes of water Ti-OH | 1600-1650 (s) |
| N-H bending | 1600 (m) |
| Ti-O vibrations | ~ 600 (s) |

### 3.4 SEM/EDX analysis

The SEM micrographs in figure 8 reveal the morphological differences between undoped $TiO_2$ (panels a–b) and N-doped $TiO_2$ nanoparticles (panels c–f). The undoped $TiO_2$ (a–b) consists of uniformly distributed, nearly spherical particles forming compact aggregates. This spherical morphology is commonly observed in $TiO_2$ nanoparticles synthesized under controlled conditions. In contrast, the N-doped $TiO_2$ (c–f) displays a more open, loosely packed network of smaller, irregularly

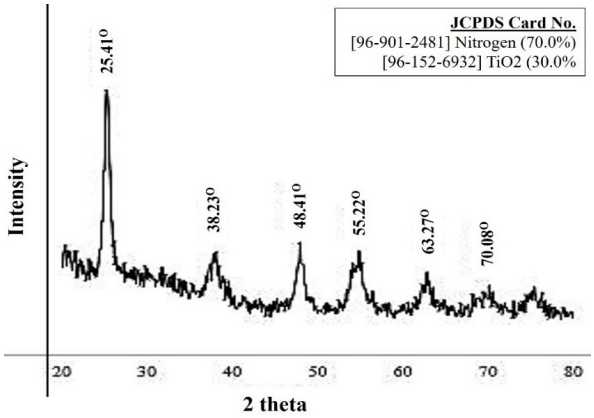


**Figure 7.** XRD pattern of N-$TiO_2$ nanoparticles.

**Table 3.** Crystallite size Calculation from XRD data for $TiO_2$.

| $2\theta$ | (h k l) | $d$ (Å) | FWHM | Element | $D$ (nm) |
|---|---|---|---|---|---|
| 25.48 | (1 0 1) | 3.495 | 0.34 | $TiO_2$ | 22.78 |
| 37.26 | (0 1 3) | 2.413 | 0.34 | $TiO_2$ | 22.13 |
| 38.2 | (0 0 4) | 2.355 | 0.34 | $TiO_2$ | 22.07 |
| 48.41 | (2 0 0) | 1.880 | 0.34 | $TiO_2$ | 21.30 |
| 54.48 | (1 0 5) | 1.684 | 0.34 | $TiO_2$ | 20.77 |
| 55.43 | (2 1 1) | 1.657 | 0.34 | $TiO_2$ | 20.68 |
| 63.27 | (0 2 4) | 1.4697 0.34 | $TiO_2$ | 19.89 | |
| Average Crystallite Size (nm) | | | | | 21.37 |

**Table 4.** Crystallite size Calculation from XRD data for N-$TiO_2$.

| $2\theta$ | (h k l) | $d$ (Å) | FWHM | Element | $D$ (nm) |
|---|---|---|---|---|---|
| 22.3 | (1 0 0) | 3.986 | 0.12 | N | 64.92 |
| 25.41 | (1 0 1) | 3.505 | 0.12 | $TiO_2$ | 64.55 |
| 27.41 | (1 1 1) | 3.254 | 0.12 | N | 64.29 |
| 31.65 | (2 0 0) | 2.827 | 0.12 | N | 63.66 |
| 38.23 | (0 0 4) | 2.354 | 0.12 | $TiO_2$ | 62.52 |
| 38.88 | (0 0 4) | 2.316 | 0.12 | $TiO_2$ | 62.40 |
| 39.1 | (2 1 1) | 2.304 | 0.12 | N | 62.36 |
| 45.41 | (2 2 0) | 1.997 | 0.12 | N | 61.04 |
| 48.24 | (2 0 0) | 1.886 | 0.12 | $TiO_2$ | 60.39 |
| 49.24 | (2 1 2) | 1.886 | 0.12 | N | 60.16 |
| 53.75 | (3 0 1) | 1.705 | 0.12 | N | 59.02 |
| 55.22 | (2 1 1) | 1.663 | 0.12 | $TiO_2$ | 58.64 |
| 63.27 | (0 2 4) | 1.469 | 0.12 | $TiO_2$ | 56.34 |
| 66.09 | (4 0 0) | 1.413 | 0.12 | N | 55.47 |
| Average Crystallite Size (nm) | | | | | 61.25 |

faceted particles (~ 45 – 83 nm). In figure 8 (c) (scale bar = 0.5 µm) and (d) (scale bar = 1 µm), the N-$TiO_2$ sample displays a porous, sponge-like network of loosely

https://dx.doi.org/10.57647/j.ijnd.2026.1701.07

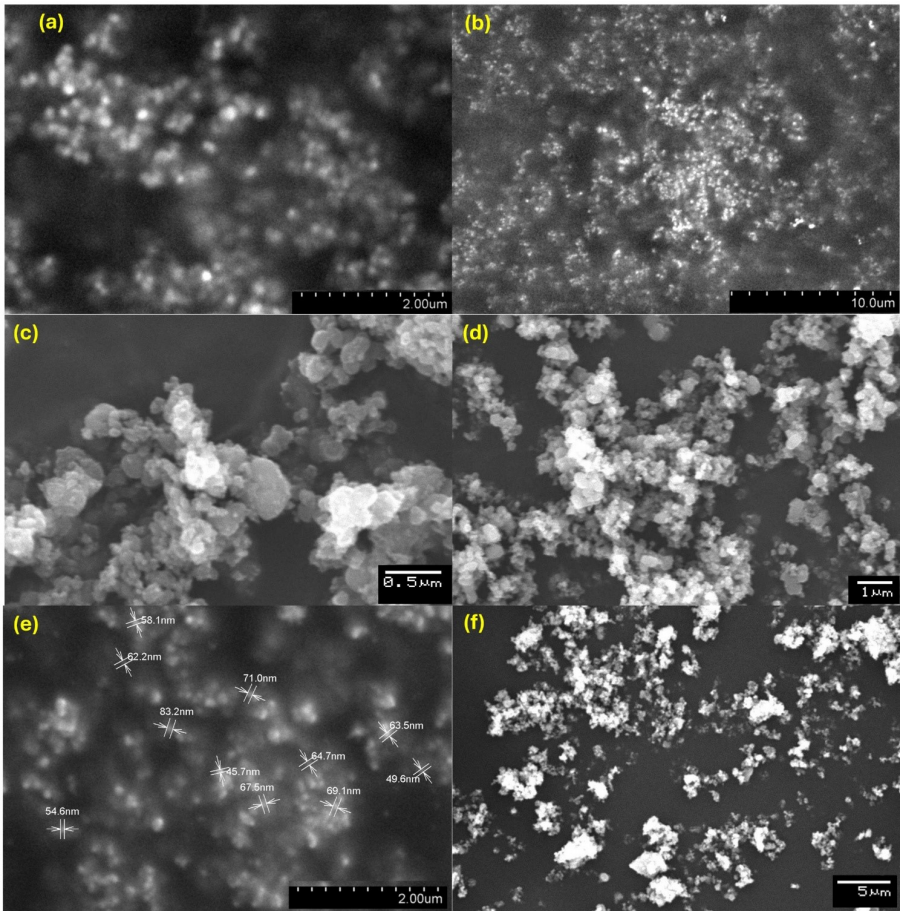


**Figure 8.** SEM images of $TiO_2$ nanoparticles (a) 2 µm, (b) 10 µm; N-$TiO_2$ nanoparticles, (c) 0.5 µm, (d) 1 µm, (e) 2 µm, (f) 5 µm at various magnifications.

connected primary particles. Panel (e) (scale bar = 2 µm) includes measured particle diameters, which range from approximately 45 to 83 nm, confirming that N-$TiO_2$ crystallites are well within the nanometer regime and are substantially smaller and more uniform than the bulk aggregates observed for undoped $TiO_2$. This enhanced porosity and reduced particle size are expected to improve pollutant adsorption and charge-carrier separation under visible-light irradiation.

The EDX analysis is shown in figure 9 (a) confirms the presence of Ti and O in the synthesized sample, and figure 9 (b) confirms the presence of Ti, O, and the addition of N in the synthesized sample. Thus, it is confirmed that Nitrogen has successfully doped into the $TiO_2$ crystal structure.

### 3.5 Application of $TiO_2$ and N-$TiO_2$ to treat pharmaceutical wastewater by adsorption

Spectrophotometric measurements at $\lambda_{max=310}$ nm were conducted on samples collected at various time intervals to determine their percentage absorbance, and a comparison graph of adsorption followed by photocatalysis for both doped and undoped nanoparticles is illustrated in figure 10. These measurements were used to calculate

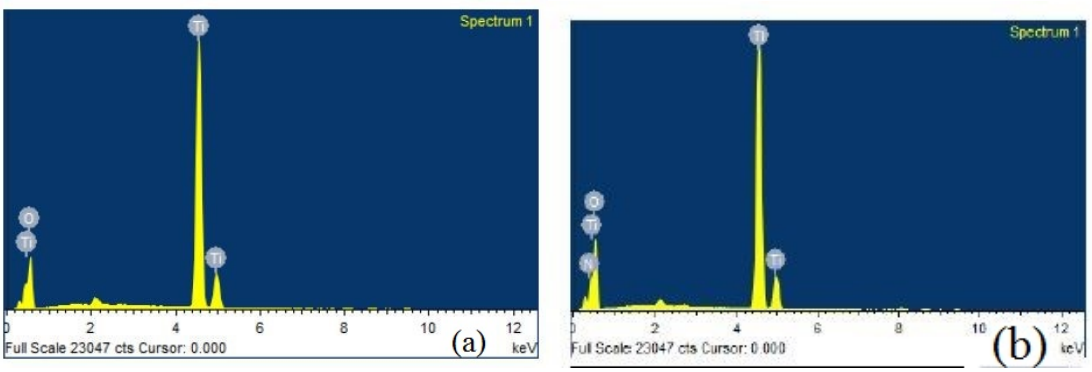


**Figure 9.** (a) EDX image of $TiO_2$ nanoparticles;(b) EDX image of N-$TiO_2$ nanoparticles.

https://dx.doi.org/10.57647/j.ijnd.2026.1701.07

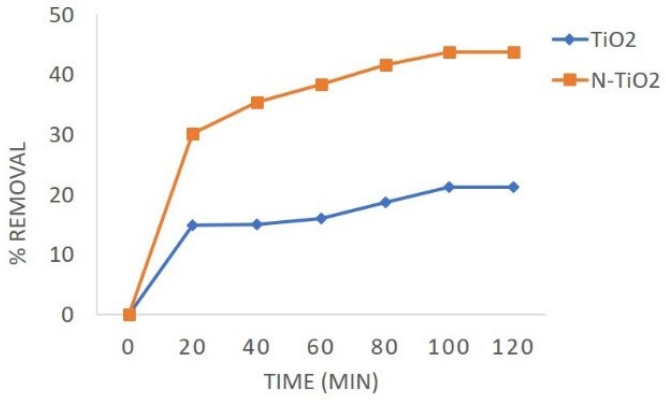


**Figure 10.** Comparison of % removal/adsorption with time for $TiO_2$ and N-$TiO_2$, 0.2 g dosage.

$'q'$ values at different time points, with the value of $q_t$ at equilibrium time (120 min) designated as $q_e$. The best-fitting model for the system was then identified by using the pseudo-first-order and second-order kinetic models.

### 3.5.1 *Adsorption kinetics: Kinetic study for $TiO_2$*

Samples were analyzed using spectrophotometry at a wavelength of 310 nm at various time intervals to measure their percent absorbance. These data were then used to calculate $'q'$ values as a function of time, with the equilibrium adsorption capacity ($q_e$) determined at 120 minutes. Both pseudo-first-order and pseudo-second-order models were used for experimental data to evaluate the adsorption kinetics, enabling the identification of the model that best describes the system's behavior.

A pseudo-first-order kinetic model is given by:

$$\ln(q_e - q_t) = \ln(q_e) - (k_1 \times t) \tag{3}$$

From figure 11 (a), this expression, $q_e$ and $q_t$ denote the quantities of pharmaceuticals adsorbed from the solution (mL/g) at equilibrium at a specific time $t$, respectively. The rate constant is represented by $k_1$ [40].

A pseudo-second-order kinetic model is given by,

$$\frac{t}{q_t} = \frac{1}{k^2 \times q_{e2}} + \frac{t}{q_e} \tag{4}$$

In this case from figure 11 (b), $k_2$ represents the rate constant, and $q_e$ and $q_t$ are the amounts of pharmaceuticals adsorbed at equilibrium and time $t$, respectively. Analysis of the data from Table 5 reveals that the theoretical $q_e$ value for the pseudo-first-order equation is

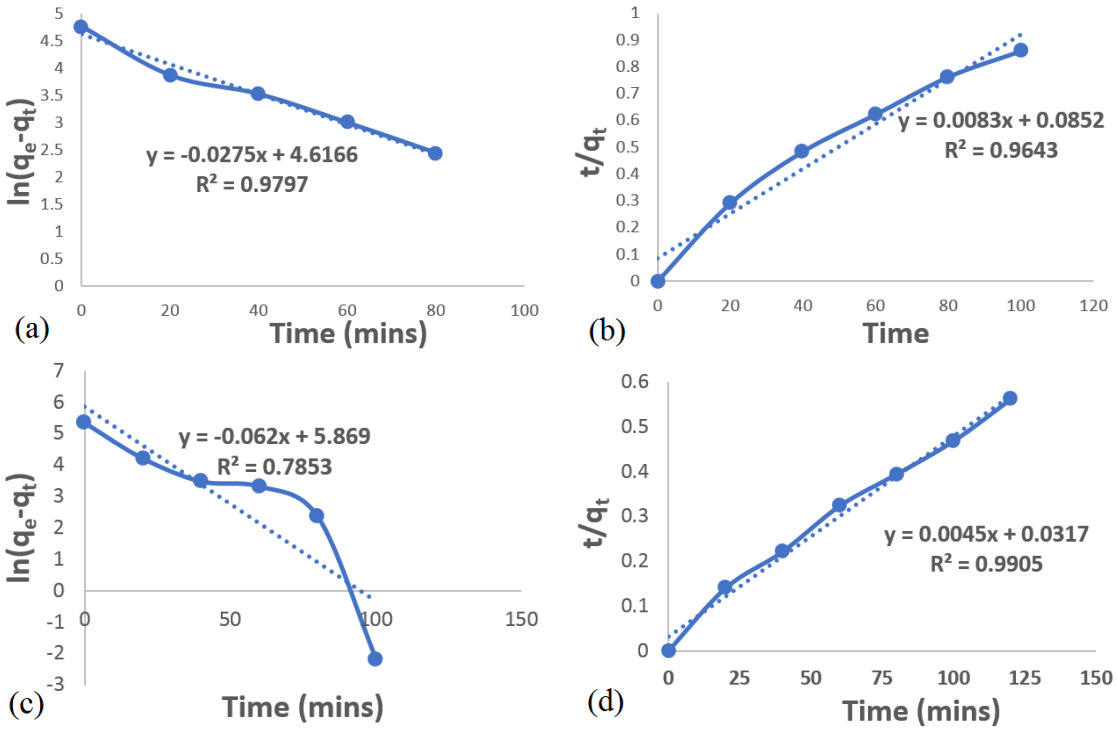


**Figure 11.** (a) Pseudo 1st order study for $TiO_2$; (b) Pseudo 2nd order study for $TiO_2$; (c) Pseudo 1st order study for N-$TiO_2$; (d) Pseudo 2nd order study for N-$TiO_2$.

https://dx.doi.org/10.57647/j.ijnd.2026.1701.07

**Table 5.** Parameters of pseudo 1st and 2nd order kinetics for $TiO_2$.

| $C_i$ (v/v%) | $Q_{e,exp}$ (mg/g in v/v%) | $Q_{e,cal}$ (mg/g in v/v%) | $K_1$ ($min^{-1}$) | $R_{12}$ | $K_2$ | $R_{22}$ |
|---|---|---|---|---|---|---|
| 100 | 116.56 | 116.59 | 0.0289 | 0.9893 | 0.000277 | 0.9863 |

closely aligned with the experimental value. Additionally, the coefficient of determination ($R_2$) for this model is notably high. On the other hand, the pseudo-second-order equation's $R_2$ value is significantly lower than the pseudo-first-order models. Based on these findings, the pseudo-first-order kinetic model provides the best fit for the experimental data. This conclusion is supported by the close agreement between theoretical and experimental $q_e$ values and the higher $R_2$ value, indicating a stronger correlation between the model and the observed data.

### *3.5.2 Adsorption kinetics: Kinetic study for N-TiO$_2$*

To kinetic analysis for N-$TiO_2$ is conducted and the results are presented in Table 6, following a comparable approach to that used for $TiO_2$ was employed. Absorbance measurements were taken at the maximum wavelength ($\lambda_{max}$) of 310 nm, with the system reaching equilibrium after 120 minutes. To determine the best fit for the experimental data, the kinetic behavior was evaluated using pseudo-first-order and pseudo-second-order models.

The pseudo-second-order model provided the best fit with $R_2^2$ = 0.9976 (see figure 11 (c) and figure 11 (d), suggesting chemisorption as the rate-limiting step. This implies that the adsorption rate depends more on available adsorption sites than on adsorbate concentration in the bulk solution.

## 3.6 Application of $TiO_2$ and N-$TiO_2$ to treat pharmaceutical wastewater by photocatalysis

After adsorption, the treated samples were exposed to sunlight for 3 hours. Samples were collected at 30-minute intervals, and their percentage absorbance values were estimated at their maximum absorbance using a UV-Vis Spectrometer, the results are illustrated in figure 12. The water quality parameters before and after treatment of the pharmaceutical wastewater, along with relevant water quality standards, are presented in Table 7. N-doped $TiO_2$ nanoparticles significantly reduced the concentrations of pH, TDS, Salinity, and Chlorides in water when compared to undoped $TiO_2$. It is observed that the treated water is within the discharge limits according to Indian Permissible water quality standards and is safe enough to dispose of treated water to surface waters. Moreover, Rao et al. (2025) demonstrated that $TiO_2$ and N-$TiO_2$ supported on various carbon nanostructures not only remove chemical contaminants but also achieve rapid microbial disinfection completely inactivating *Escherichia coli* under UV-visible light highlighting their dual utility in comprehensive water purification [39].

**Table 6.** Parameters of pseudo 1st and 2nd order kinetics for N-$TiO_2$.

| $C_i$ (v/v%) | $Q_{e,exp}$ (mg/g in v/v%) | $Q_{e,cal}$ (mg/g in v/v%) | $K_1$ ($min^{-1}$) | $R_{12}$ | $K_2$ | $R_{22}$ |
|---|---|---|---|---|---|---|
| 100 | 116.56 | 116.59 | 0.0289 | 0.9893 | 0.000277 | 0.9863 |

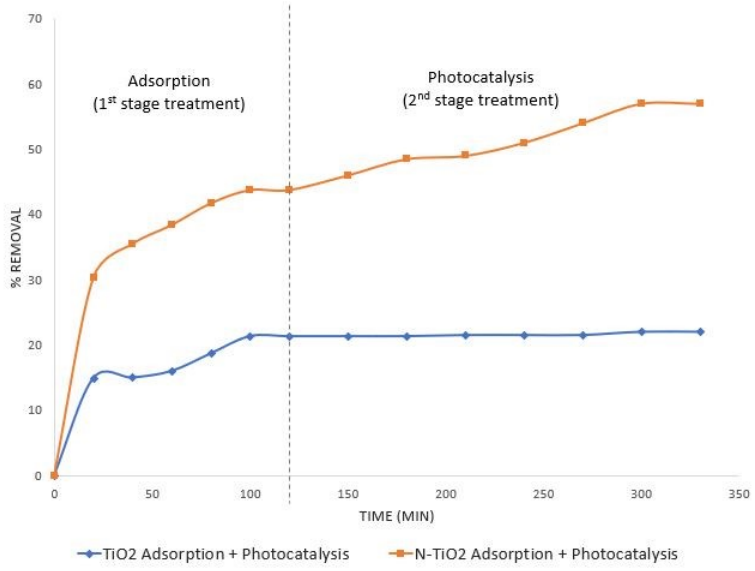


**Figure 12.** Total % removal of Industrial Pharmaceutical effluent $TiO_2$ and N-$TiO_2$ by Adsorption followed by Photocatalysis-Comparison Graph.

https://dx.doi.org/10.57647/j.ijnd.2026.1701.07

**Table 7.** Water quality standards-before and after treatment.

| Parameters | Raw Pharma effluent | $TiO_2$, Adsorption | $TiO_2$, Photocatalysis | N-$TiO_2$, Adsorption | N-$TiO_2$, Photocatalysis | Indian Drinking Water Quality Std.s [2012] | Indian Permissible Water Quality Std.s [2012] |
|---|---|---|---|---|---|---|---|
| pH | 9.2 | 8.5 | 8.5 | 7.5 | 7.5 | 6.5-8.5 | No Relaxation |
| TDS (ppm) | 3780 | 3074 | 3009 | 1926 | 1326 | < 500 | < 2000 |
| Salinity (ppt) | 4.1 | 3.3 | 3.2 | 2.0 | 1.3 | – | – |
| Chlorides (ppm) | 2345.81 | 1880.44 | 1838.02 | 1143.37 | 770.45 | < 250 | < 1000 |

## 4. Conclusion

In this study, $TiO_2$ and N-doped $TiO_2$ nanoparticles were successfully synthesized and characterized using UV-visible spectroscopy, XRD, FTIR, SEM, DLS, and EDX techniques. These nanomaterials were applied for the treatment of pharmaceutical industrial wastewater by combining adsorption-photocatalysis approach. During the adsorption phase, N-$TiO_2$ demonstrated a superior performance, by reducing the pollutant concentration to 43.77%, compared to 21.34% for undoped $TiO_2$. The enhanced performance is attributed to the increased surface area and improved surface characteristics of the doped material. Subsequent photocatalytic treatment with N-$TiO_2$ further decreased pollutant levels to 57%, whereas $TiO_2$ achieved only a 22% reduction under the same conditions. According to kinetic analysis, $TiO_2$ and N-$TiO_2$ followed pseudo-first-order and pseudo-second-order adsorption kinetics, respectively, suggesting distinct adsorption mechanisms arising from differences in surface properties. N-$TiO_2$ also outperformed undoped $TiO_2$ in pseudo-first-order photocatalytic degradation, owing to its narrower band gap and greater visible-light absorption, which enhanced charge separation and the generation of reactive species. These findings clearly demonstrate the effectiveness of nitrogen doping in enhancing the photocatalytic and adsorptive properties of $TiO_2$ nanoparticles. However, further studies are needed to assess the long-term stability and reusability of the catalyst under real-world conditions. Given its potential for solar-driven water treatment, the use of N-$TiO_2$ under natural sunlight represents a viable and sustainable strategy for the remediation of pharmaceutical wastewater.

**Acknowledgement**
The authors extend gratitude to the Head of the Chemical Engineering department at JNTUA College of Engineering Anantapur, for granting access to the essential facilities required for the experimental work. Furthermore, the authors thank the valuable support provided by OTRI-JNTUA, Savitribai Phule Pune University, and Osmania University (OU) in Hyderabad for offering a range of analytical tools that were instrumental in the characterization and analysis of the prepared samples.

**Authors contributions**
Authors have contributed equally in preparing and writing the manuscript.

**Availability of data and materials**
The authors declare that the data supporting the findings of this study are available within the paper.

**Conflict of interests**
The authors assert that they do not have any identifiable conflicting financial interests or personal relationships that might be perceived to influence the work presented in this paper.

### References

1. Abdul-Raheim AM, M ES, K FR, and E AM. "Low cost biosorbents based on modified starch iron oxide nanocomposites for selective removal of some heavy metals from aqueous solutions." Advanced Materials Letters 2016; 7:402–409. DOI: 10.5185/amlett.2016.6061
2. Amin MT, Alazba AA, and Manzoor U. "A Review of Removal of Pollutants from Water/Wastewater Using Different Types of Nanomaterials." Advances in Materials Science and Engineering 2014; 2014:1–24. DOI: 10.1155/2014/825910
3. Munzhelele EP, Mudzielwana R, Ayinde WB, and Gitari WM. "Pharmaceutical contaminants in wastewater and receiving water bodies of South Africa: A review of sources, pathways, occurrence, effects, and geographical distribution." Water 2024; 16:796. DOI: 10.3390/w16060796
4. Valdez HA, Jiménez GG, Granados SG, and De León CP. "Degradation of paracetamol by advanced oxidation processes using modified reticulated vitreous carbon electrodes with $TiO_2$ and $CuO/TiO_2/Al_2O_3$. " Chemosphere 2012; 89:1195–1201. DOI: 10.1016/j.chemosphere.2012.07.020
5. Ortúzar M, Esterhuizen M, Olicón-Hernández DR, González-López J, and Aranda E. "Pharmaceutical Pollution in Aquatic Environments: A Concise review of environmental impacts and bioremediation systems." Frontiers in Microbiology 2022; 13. DOI: 10.3389/fmicb.2022.869332
6. Chekir N, Laoufi NA, and Bentahar F. "Spiramycin photocatalysis under artificial UV radiation and natural sunlight." Desalination and Water Treatment

2013; 52:6832–6839. DOI: 10.1080/19443994.2013.821632

7. Rajendran R, Abirami M, Prabhavathi P, Premasudha P, Kanimozhi B, and Manikandan A. "Biological treatment of drinking water by chitosan based nanocomposites." African Journal of Biotechnology 2015; 14:930–936. DOI: 10.5897/ajb2015.14469
8. Czech B and Buda W. "Multicomponent nanocomposites for elimination of diclofenac in water based on an amorphous $TiO_2$ active in various light sources." Journal of Photochemistry and Photobiology a Chemistry 2016; 330:64–70. DOI: 10.1016/j.jphotochem.2016.07.024
9. Arunpandian M, Selvakumar K, Raja A, Rajasekaran P, Thiruppathi M, Nagarajan E, and Arunachalam S. "Fabrication of novel $Nd_2O_3$/ZnO-GO nanocomposite: An efficient photocatalyst for the degradation of organic pollutants." Colloids and Surfaces a Physicochemical and Engineering Aspects 2019; 567:213–227. DOI: 10.1016/j.colsurfa.2019.01.058
10. Xue X, Cheng R, Shi L, Ma Z, and Zheng X. "Nanomaterials for water pollution monitoring and remediation." Environmental Chemistry Letters 2016; 15:23–27. DOI: 10.1007/s10311-016-0595-x
11. Obare SO and Meyer GJ. "Nanostructured materials for environmental remediation of organic contaminants in water." Journal of Environmental Science and Health Part A 2004; 39:2549–2582. DOI: 10.1081/ese-200027010
12. M A, K S, A R, P R, C R, ER N, A P, and S A. "Rational design of novel ternary $Sm_2WO_6$/ZnO/GO nanocomposites: An affordable photocatalyst for the mitigation of carcinogenic organic pollutants." Colloids and Surfaces a Physicochemical and Engineering Aspects 2020; 596:124721. DOI: 10.1016/j.colsurfa.2020.124721
13. Armaković SJ, Savanović MM, and Armaković S. "Titanium dioxide as the most used photocatalyst for water purification: an overview." Catalysts 2022; 13:26. DOI: 10.3390/catal13010026
14. Zoubi WA, Al-Hamdani AaS, Sunghun B, and Ko YG. "A review on $TiO_2$-based composites for superior photocatalytic activity. " Reviews in Inorganic Chemistry 2021; 41:213–222. DOI: 10.1515/revic-2020-0025
15. Huang F, Yan A, and Zhao H. "Influences of doping on photocatalytic properties of $TiO_2$ photocatalyst." 2016; InTech eBooks. DOI: 10.5772/63234
16. Sendão RMS, Da Silva JCGE, and Da Silva LP. "Photocatalytic removal of pharmaceutical water pollutants by $TiO_2$–Carbon dots nanocomposites: A review." Chemosphere 2022; 301:134731. DOI: 10.1016/j.chemosphere.2022.134731
17. Ghasemi S, Parastesh A, Padervand M, Ren H, Li X, Labidi A, Signoretto M, Dawi EA, Hamzehlouyan T, Lichtfouse E, and Wang C. "Recent progress on Z- and S-scheme photocatalysis: mechanistic understanding toward green applications." Current Opinion in Chemical Engineering 2024; 47:101059. DOI: 10.1016/j.coche.2024.101059
18. Ren H, Miao Z, Zhao Y, Ghasemi S, Feng X, Liu E, and Padervand M. "Advances and challenges in multiple s-scheme heterojunction photocatalysts." Journal of Alloys and Compounds 2025 :180646. DOI: 10.1016/j.jallcom.2025.180646
19. Aswini R, Padmanaban A, Vigneshwaran S, Valdes H, and Arunachalam S. "A review on versatile nano-photocatalysts for environmental remediation: Carbon-decorated bismuth-based nanomaterials." Nano-Structures & Nano-Objects 2023; 35:100991. DOI: 10.1016/j.nanoso.2023.100991
20. Arunpandian M, Sivaganesh D, Revathy MS, Selvakumar K, Arunachalam S, and Geetha D. "Facile synthesis of spherically $SrWO_4$ nanomaterials via surfactant-assisted co-precipitation method: an affordable catalyst for the mitigation of carcinogenic organic dye." International Journal of Environmental & Analytical Chemistry 2020; 102:5738–5755. DOI: 10.1080/03067319.2020.1803847
21. Zhou H, Wang H, Yue C, He L, Li H, Zhang H, Yang S, and Ma T. "Photocatalytic degradation by $TiO_2$-conjugated/coordination polymer heterojunction: Preparation, mechanisms, and prospects." Applied Catalysis B Environment and Energy 2023; 344:123605. DOI: 10.1016/j.apcatb.2023.123605
22. Ramalingam G, Pachaiappan R, Kumar PS, Dharani S, Rajendran S, Vo DN, and Hoang TK. "Hybrid metal organic frameworks as an Exotic material for the photocatalytic degradation of pollutants present in wastewater: A review." Chemosphere 2021; 288:132448. DOI: 10.1016/j.chemosphere.2021.132448
23. Azari B, Pourahmad A, Sadeghi B, and Mokhtary M. "Green synthesis of $SiO_2$ from Equisetnm arvense plant for synthesis of $SiO_2$/ZIF-8 MOF nanocomposite as photocatalyst." Journal of Coordination Chemistry 2023; 76:219–231. DOI: 10.1080/00958972.2023.2166408
24. Balu S, Ganapathy D, Arya S, Atchudan R, and Sundramoorthy AK. "Advanced photocatalytic materials based degradation of micropollutants and their use in hydrogen production – a review." RSC Advances 2024; 14:14392–14424. DOI: 10.1039/d4ra01307g

25. Labidi A, Ren H, Liang X, Dong Q, Li X, Tian Q, Sial A, Cui Y, Kang H, Liang J, Zhao K, Lichtfouse E, Padervand M, and Wang C. "Visible–light–driven photocatalytic degradation of ciprofloxacin antibiotic by novel heterostructured coal fly ash waste: Mechanism insight, toxicity pathway and DFT calculation." Materials Today Chemistry 2024; 42:102388. DOI: 10.1016/j.mtchem.2024.102388

26. Pourjafari M, Ghane M, Kaboosi H, Sadeghi B, and Rezaei A. "Antibacterial Properties of Ag–Cu Alloy Nanoparticles Against Multidrug-Resistant Pseudomonas aeruginosa Through Inhibition of Quorum Sensing Pathway and Virulence-Related Genes." Journal of Biomedical Nanotechnology 2022; 18:1196–1204. DOI: 10.1166/jbn.2022.3331

27. Khodadad H, Hatamjafari F, Pourshamsian K, and Sadeghi B. "Microwave-assisted Synthesis of Novel Pyrazole Derivatives and their Biological Evaluation as Anti-Bacterial Agents." Combinatorial Chemistry & High Throughput Screening 2020; 24:695–700. DOI: 10.2174/1386207323666201019152206

28. Yueyu S. "The synergistic degradation of pollutants in water by photocatalysis and PMS activation." Water Environment Research 2023; 95. DOI: 10.1002/wer.10927

29. Liu Y, Dai X, Li J, Cheng S, Zhang J, and Ma Y. "Recent progress in $TiO_2$–biochar-based photocatalysts for water contaminants treatment: strategies to improve photocatalytic performance." RSC Advances 2024; 14:478–491. DOI: 10.1039/d3ra06910a

30. Labidi A, Ren H, Sial A, Wang H, Liang X, Liang J. PM, Lichtfouse E, and Wang C. "Organic radicals used to modify materials surface and their application to remove pharmaceutical residues from wastewater." 2024; Elsevier eBooks:321–339. DOI: 10.1016/b978-0-443-13346-6.00012-9

31. Cunha RF, Da Silva TF, Cavalcante RP, De Melo Da Silva L, Nazario CED, Wender H, Casagrande GA, De Oliveira LCS, Marco P, Giménez J, Sirés I, Machulek A, and Junior De Oliveira SC. "Development of $TiO_2$-based photocatalysts with high photocatalytic activity under simulated solar light: Metoprolol degradation and optimization via Box-Behnken." Catalysis Today 2013; 432:114607. DOI: 10.1016/j.cattod.2024.114607

32. Gurramkonda N, Staderini E, and Tumma B. "Synthesis of Bio-Inspired self-cleaning hydrophobic surfaces using ZNO nanoparticles." Mechanisms and Machine Science 2024 :463–475. DOI: 10.1007/978-3-031-63755-1_34

33. Chandan AK, Mallika GN, and Narsaiah TB. "A green approach to arsenic removal using ZnO nanoparticles synthesized from Acacia Catechu leaf extract." Materials Today Proceedings 2022; 72:110–119. DOI: 10.1016/j.matpr.2022.06.199

34. Mallika GN and Narsaiah TB. "Synthesis of $TiO_2$ Nanoparticles using Sol-Gel Method for the Treatment of Pharmaceutical Wastewater." 2017. Available from: https://www.ijsrd.com/articles/IJSRDV5I60128.pdf

35. Behara DK, Alugoti DVP, and Sree PP. "Multi element doped type-II heterostructure assemblies (N, S- $TiO_2$/ZnO) for electrochemical crystal violet dye degradation." International Journal of Nanodimension 2020; 11:303–311. Available from: http://www.ijnd.ir/article_675538_f5ac92b522d5551d1b6889b7233deec6.pdf

36. Biziuk M, Beyer A, and Zukowska J. "Preservation and storage of water samples." Analytical Chemistry Series 2009 :19–39. DOI: 10.1201/9781420082692-c2

37. Borges M, Sierra M, Cuevas E, García R, and Esparza P. "Photocatalysis with solar energy: Sunlight-responsive photocatalyst based on $TiO_2$ loaded on a natural material for wastewater treatment. " Solar Energy 2016; 135:527–535. DOI: 10.1016/j.solener.2016.06.022

38. Shathy RA, Fahim SA, Sarker M, Quddus MS, Moniruzzaman M, Masum SM, and Molla MaI. "Natural sunlight driven photocatalytic removal of toxic textile dyes in water using B-Doped ZNO/$TiO_2$ nanocomposites." Catalysts 2022; 12:308. DOI: 10.3390/catal12030308

39. Rao MS, Tiwari A, Sethi D, Dash T, Sankaran KJ, and Sakthivel R. "Effect of various carbon supports for $TiO_2$ and N-doped $TiO_2$ photocatalysts for inactivation of Escherichia coli in water under UV–visible light." Journal of Photochemistry and Photobiology B Biology 2025; 268:113180. DOI: 10.1016/j.jphotobiol.2025.113180

40. Raghupathy D, Ramgopal G, and Ravikumar C. "Photocatalytic degradation of direct green & fast orange red dyes: Electrochemical sensor of lead using cupric oxide nanoparticles synthesized via sonochemical route." Sensors International 2022; 3:100204. DOI: 10.1016/j.sintl.2022.100204